Arguments for Keeping Uniform Alumina Concentration and Anode-Cathode Distance in Aluminium Electrolysis Cells

Asbjørn Solheim
Chief Scientist
SINTEF Industry, P.O. Box 4760 Torgarden, NO-7465 Trondheim, Norway
Corresponding author: asbjorn.solheim@sintef.no
https://doi.org/10.71659/icsoba2024-al015

Abstract

Four main topics related to non-uniformity in aluminium electrolysis cells are treated in this paper. i) The alumina concentration can vary by 2 wt% throughout the bath, which is the root cause of the low voltage anode effect (LVAE). By using a statistical method, a general chart separating the fields for LVAE and high voltage anode effect (HVAE) could be derived. Both types of AE occur at higher average alumina concentration when the concentration is less uniform. ii) Anodic current distribution can be used as a rough measure of the standard deviation in the anode-cathode distance (ACD); e.g., 12 % standard deviation for the current distribution corresponds to 5 mm standard deviation for the ACD. It is suggested that variation in ACD is caused by perturbation of the metal pool surface each time anodes are replaced due to Lorentz forces and bath density variations. iii) A simple formula for the effect on local ACDs by local bath density variations due to non-uniform alumina concentration was derived. It was shown that the time for equalisation of individual ACDs by current dependent anode wear is longer than the time between anode shifts. This entails that the ACD always varies with time and position. iv) Non-uniform ACD may be detrimental to the current efficiency (CE) because gas bubbles and metal waves can contact each other underneath anodes with low ACD. The effect is more severe when the average ACD is low.

Keywords: Alumina, Anode-cathode distance, Anode effect, Current efficiency.

1. Introduction

The alumina concentration in the electrolysis bath varies significantly with time and position. The concentration in samples taken simultaneously at different locations can vary by at least 2 wt% [1-3]. The variation affects the onset of anode effect, the individual anode-cathode distances (local ACD), the anodic current distribution, and the current efficiency (CE). These items are all related to the alumina distribution.

During anode effect perfluorocarbons (PFCs) evolve (tetrafluoromethane, CF_4 and hexafluoro-ethane, C_2F_6). The PFC generation due to the "classic" high voltage anode effect (HVAE) has been significantly reduced during the last three decades [4]. The first news about PFC evolution during apparently normal electrolysis stems from a report by the Research Institute of Chalco in 2009 [5]. It turned out that this was caused by a "new" class of AE, today termed LVAE. The LVAE is strongly linked to the alumina distribution. Methods for calculation and consistent reporting of PFC from LVAE are still being developed [6].

It has been substantiated [7, 8] that changes in local bath density due to variable alumina concentration affect the local bath depth, and thereby the local ACD. While it is generally accepted that the metal-bath interface is curved due to magnetic forces, the present author has experienced that many are sceptical about a similar effect of density variations – perhaps because it feels intuitively wrong that a liquid-liquid interface should be non-horizontal in absence of external forces. Moreover, the effect of variable density in a system of two immiscible liquids is

not treated in common textbooks. The effect is the same as when the sea level increases locally due to low atmospheric pressure.

It was suggested that the CE may become low due to direct contact between metal waves and gas bubbles at low ACD [9]. Too large variation in ACD will then be detrimental to the CE because several anodes will be below the critical limit where the metal loss becomes significant. The present paper does not contain radical or new thoughts, and most of the contents has been published earlier [7-10]. Still, it may be useful to take a step back and contemplate several pieces in the puzzle to see the entire picture. The main purpose is to demonstrate how non-uniformity brings about several adverse effects, which can be estimated by statistical methods.

2. A Statistical View on Anode Effects

2.1 Theoretical Treatment

A statistical analysis of the anode effect was recently published [10]. The idea was that the regions of LVAE and HVAE could be estimated from the mean alumina concentration and the standard deviation. A summary of the calculations and results is given in the following.

The anode effect starts when the alumina concentration at the anode surface becomes virtually zero, resulting in the formation of a non-conducting CF_x film blocking of the current at a part of the anode. If the rest of the anode can handle the increased current density, the AE will remain local (LVAE). If not, the AE will spread rapidly to the entire anode (HVAE) as explained by Thonstad et al. [11]. An LVAE can take place not only at entire single anodes, but also locally on a part of a single anode block. If the LVAE affects a significant part of an anode, it can be detected in prebake cells equipped with individual anode current measurement [12]. However, it will be difficult to discover if only a minor area is affected. Söderberg cells probably also have LVAEs, due to their highly irregular surface on the bottom of the anode, but they are even harder to reveal.

Alumina is transported to the anode by diffusion (ordinary mass transfer). The "critical" alumina concentration (c_c) is the bulk concentration when the surface concentration becomes zero. When the current is blocked at an area fraction of the anode (a_{AE}), c_c increases at other parts of the anode:

$$c_c = \frac{c_c^0}{1 - a_{AE}} \tag{1}$$

If there is enough alumina elsewhere, only the passivated part of the anode will be affected. The possible spreading of the AE depends on the concentration distribution, and the problem therefore lends itself to statistical treatment.

The alumina concentration (c) has a mean value (c_m), a standard deviation (σ), and a certain probability distribution (p) around the mean value. The familiar Gaussian "bell curve" was used, which has the probability distribution formula:

`

$$p = \frac{1}{\sigma\sqrt{2\pi}} \cdot \exp\left\{-\frac{1}{2}\left(\frac{c - c_m}{\sigma\sqrt{2}}\right)^2\right\} \tag{2}$$

The cumulative distribution (a) represents the area underneath the probability distribution curve at a certain c, in our case the fraction of the anode that is at AE (erf is the error function):

$$a_{AE} = \frac{1}{2} \cdot \left\{ 1 + \mathrm{erf}\left(\frac{c_c - c_m}{\sigma\sqrt{2}} \right) \right\} \quad (3)$$

The mean alumina concentration at given a_{AE} and σ could be calculated from the above equations. As an example: If 5 % of the anode is at AE (a_{AE} = 0.05) and c_c^0 = 0.8 wt%, Equation 1 gives c_c = 0.842 wt%. By inserting c_c = 0.842 wt% in Equation 3 and assuming σ = 0.7 wt%, it is found by iteration that c_m = 1.994 wt% returns the value a_{AE} = 0.05. Since the difference between c_c and c_m is proportional with σ at a given a_{AE} (Equation 3), a plot of c_m as a function of σ produces a straight line that crosses the c_m-axis at $c_m = c_c^0$.

The above equations could also be used to predict the onset of a HVAE. At fixed c_m and σ, a_{AE} was calculated iteratively from Equation 3 (starting with $c = c_c^0$). By reducing c_m in very small steps, there was a final lowest c_m where the iterations did not converge.

2.2 Regions of HVAE and LVAE

The results of the calculations described above are shown in Figure 1. There is no sharp border between the "No AE" region and the "LVAE" region, but at some point, the anode area fraction on AE is so low that the PFC generation will be negligible. It was found that a_{AE} as low as 0.0001 is possible, based on numerical calculations of current distribution and anode voltage [12]. The HVAE occurs at higher average alumina concentration if the standard deviation is large.

Industrial data published by Chen et al. [2] and by Tessier et al. [3] are also shown in Figure 1. One of the data sets by Chen et al. is in the "No AE" region in Figure 1, while the other is in the "LVAE" region. The results of Tessier et al. [3] are all close to the not-so-well-defined border between "No AE" and "LVAE". However, the combination of mean value and standard deviation was well into the "LVAE" region occasionally, as judged from time series where concentrations were graphically represented by a colour scale [3].

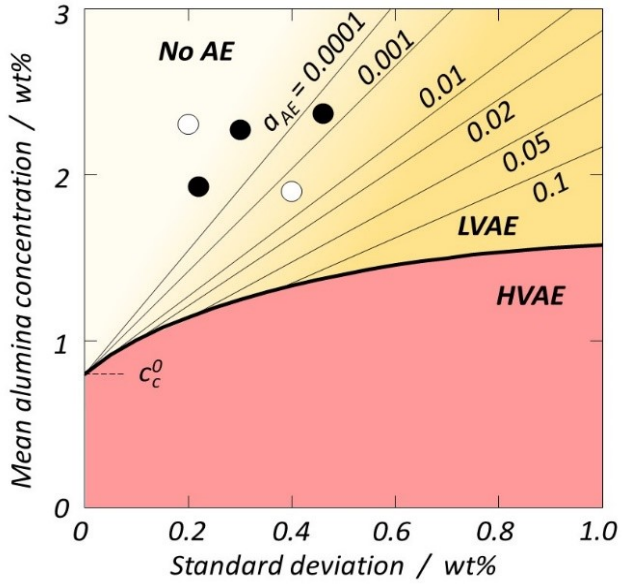

Figure 1. Regions of absence of anode effect (No AE), low voltage anode effect (LVAE), and high voltage anode effect (HVAE) in terms of the mean alumina concentration and the standard deviation. The thin lines indicate different values of the fraction of the anode area that is on LVAE. Open symbols: Industrial data by Chen et al. [2], filled symbols: Industrial data by Tessier et al. [3]. Figure redrawn after Solheim [10].

3. Alumina and Anode-Cathode Distance

3.1 Anodic Current Distribution

The anodic current distribution in aluminium electrolysis cells is normally not measured continuously, even though a lot of information can be gathered from such measurements [12]. It is not uncommon that the standard deviation in the individual anode currents is well above 10 percent of the average; in fact, numbers above 20 percent were reported by Verreault and Santerre [13] for anodes located close to the feeders and about 15 percent elsewhere. The reasons for the variation were discussed by Solheim and Moxnes [7], who used a model for predicting the effects of several factors on the anodic current distribution. It was found that the combined effect of freeze formation on newly set anodes, variable anode setting height, age-dependent vertical and horizontal anode dimensions, slots that disappear, variable alumina concentration influencing overvoltage and electrical conductivity, variable contact resistances, and position in the cell could only account for 4 percent standard deviation in the individual anode currents. The main reason for the high standard deviation appeared to be variation in the local ACD. Intuitively, this may seem odd, because low local ACD gives higher current density and increased anode wear rate, leading to a tendency towards uniform ACD and adaptation of the anode shape to the metal surface. The only possible explanation appears to be that there is a regular redistribution of the metal level, probably related to the replacement of anodes.

3.2 Current and Anode-Cathode Distance

The voltage between the anode beam and the metal pad (U_{bm}) is approximately the same for all anodes in a cell. For each anode, the beam-metal voltage is the sum of the extrapolated cell voltage E_e [1.68 V] and the product of current (I') and internal resistances. The resistance in the bath (R_b) is given by:

$$R_b = \frac{\delta}{A\kappa} \tag{4}$$

where δ is the ACD, A is the anode area (1.05 m^2), and κ is the electrical conductivity of the bath (212 $ohm^{-1}m^{-1}$ [14]). The resistance other places than in the bath (R_{ob}) comprises the anode assembly, the bubble layer, and the cathodic and anodic concentration voltages ($7 \cdot 10^{-5}$ ohm for one anode). U_{bm} is taken to be 3.728 V. The current through one anode becomes:

$$I' = \frac{U_{bm} - E_e}{\frac{\delta}{A\kappa} + R_{ob}} \quad \text{[A]} \tag{5}$$

With the data mentioned, the current is very close to 10 kA at δ = 0.03 m, which are then taken to be the average values. The calculation does not account for individual anode current variation caused by different age (height and cross-sectional area) or by variation in contact resistances. Equation 5 will be used in consecutive calculations.

To obtain an impression of the relationship between ACD variation and anodic current distribution, Equation 5 was applied for a large number of anodes where the ACD could vary around the average ACD (30 mm). Two probability distributions were employed, either the Gauss function (Equation 2), or a flat distribution where the ACD was selected as a random value between set maximum and minimum values. The resulting relationship between standard deviation in current and standard deviation in ACD is shown in Figure 2. Perhaps surprising, the choice of probability distribution for ACD played only a minor role. A standard deviation of 20

percent, as was observed by Verreault and Santerre [13], requires an ACD standard deviation of 7-8 mm, which corresponds to a max-min variation of more than 20 mm in the flat distribution model. This seems like an extreme variation, but it will be substantiated below that it is possible.

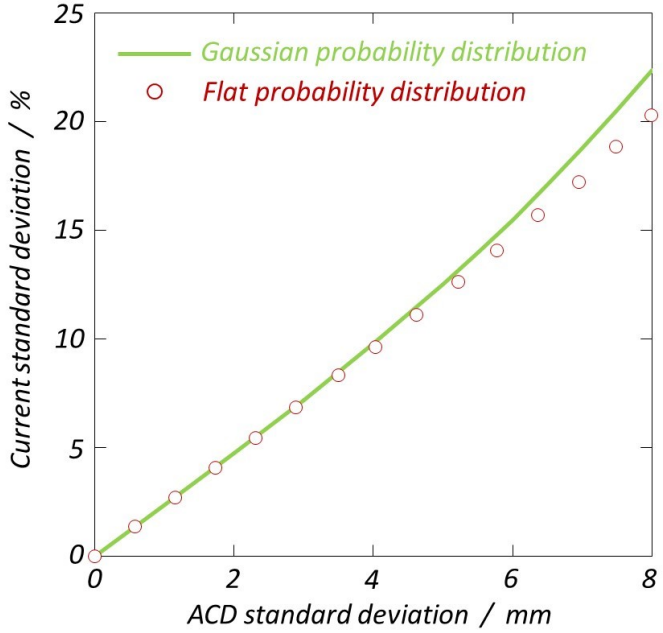

Figure 2. Standard deviation in individual anode currents as a function of standard deviation in ACD. The average values for current and ACD are 10 kA and 30 mm, respectively. Calculated with Gaussian probability distribution for ACD or a flat probability distribution. In the latter case, the standard deviation in ACD was about 30 percent of the max-min difference.

3.3 Time to Attain Constant Anode-Cathode Distance

The wear rate of the anode can be calculated by:

$$\left(\frac{dz}{dt}\right)_{wear} = \frac{I' M_C k}{4 F A \rho_C} \quad [\mathrm{m\ s^{-1}}] \tag{6}$$

where z is the vertical coordinate, t is time, M_C is the atomic mass of carbon (0.012 kg mol^{-1}), F is Faraday's constant (96 485 C mol^{-1}), ρ_C is the density of the anode carbon (1580 kg m^{-3}), and k is a dimensionless factor accounting for anode dusting and the Boudouard reaction (k = 1.04 corresponds to 14 kg C/t Al excluding airburn).

The anode is lowered at an average rate $(dz/dt)_{av}$ given by the average current. When assuming constant position of the metal-bath interface, the time-dependent variation in the ACD becomes:

$$\frac{d\delta}{dt} = \left(\frac{dz}{dt}\right)_{wear} - \left(\frac{dz}{dt}\right)_{av} = \frac{M_C k}{4 F A \rho_C} \cdot \left(I' - I'_{av}\right) \tag{7}$$

Combination with Equation 5 gives:

$$d\delta = \frac{M_C k \left(U_{bm} - E_e\right) \kappa}{4 F \rho_C} \cdot \left(\frac{1}{\delta + R_{ob} \kappa A} - \frac{1}{\delta_{av} + R_{ob} \kappa A}\right) \cdot dt \tag{8}$$

An explicit solution to Equation 8, i.e., a solution that expresses the ACD directly as a function of time, could not be found. An iterative solution, using data mentioned above, is shown in Figure 3. It can be noted that it takes longer time to restore the "normal" situation when starting from a high ACD. Higher current density decreases the time needed to approach equilibrium. The time to reach equilibrium will also be reduced with inferior anodes characterized by high losses by dusting and Boudouard reaction, leading to higher value of k in Equation 8.

From the data in the preceding section, it is necessary to conclude that the ACD in normal situations can vary by at least 20 mm between anodes. However, Figure 3 shows that all the individual ACDs will be within 10 mm after about 4 days, even when they start at extremely different levels. The logical implication is that the metal pad must undergo regular perturbations, probably induced by the anode replacements typically taking place every second day (double shift). When the cell is thrown into a new situation every second day, the individual ACDs will never come to equilibrium.

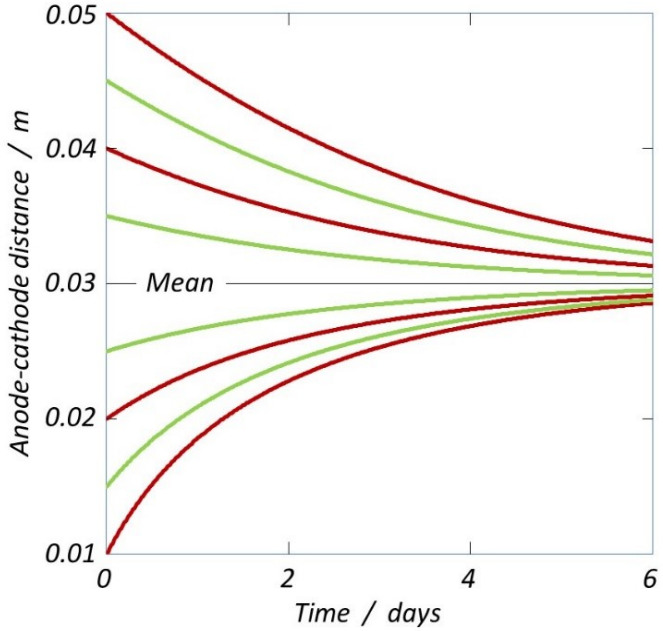

Figure 3. ACD as a function of time, calculated from Equation 8.

3.4 Variation of the Vertical Position of the Metal-Bath Interface

Kolås et al. [12] measured the current through individual anodes, and it was found that the current to the neighbouring anodes increased after an anode shift. The effect on the metal pad due to changes in the magnetic field and Lorentz forces upon setting of new anodes was modelled by Segatz et al. [15] throughout a full anode cycle. They found that the local ACD often decreased at one side of the newly set anode, while it increased at the other side. Similar findings were reported by Hue et al. [16]. It was noted that the two-phase flow pattern is changed and that the ACDs for all anodes varied. There was good agreement between modelled and measured individual anode currents.

While there is no doubt that the metal pad reacts on the changes in the magnetohydrodynamic (MHD) forces acting on it, it is also likely that local metal and bath heights are affected by dynamic pressure as well as local bath density gradients caused by variable alumina concentration [7, 8]. The latter effect resembles the variation in sea level with atmospheric pressure.

There is no reason to doubt that the alumina distribution as well as dynamic pressure caused by bath flow is influenced when setting a new anode. New anodes draw very little current, leading to redistribution of the current and thereby the alumina consumption pattern. The bath flow pattern will also change. The entire volume between a newly set anode and the metal surface will be filled with frozen bath, effectively blocking the bath flow in that region. Moreover, perturbation of the metal surface enhances the volumetric bath flow rate in some regions and restricts the flow in other parts, due to variation in the height of the cross-section available for bath flow. In other words, the consumption of alumina as well as the transport is affected.

To estimate the effect of density, the following equation was derived based on the premise that the combined weight of the bath and metal columns must be the same everywhere in the cell [8]:

$$z_{i(loc)} = z_{i(av)} \cdot \frac{\rho_m - \rho_{b(av)}}{\rho_m - \rho_{b(loc)}} \quad (9)$$

where z_i is the vertical position of the metal-bath interface (local and average values) and ρ_m and ρ_b are the densities of metal and bath, respectively. Equation 9 was applied using densities for bath [17] and molten aluminium [18]. The average bath depth was taken to be the 0.2 m and the average alumina concentration was 3.5 wt%. Figure 4 shows the local bath depth as a function of the local alumina concentration for the three bath compositions. A sudden change in alumina distribution will bring about a change in the local position of the interface. E.g., if the local alumina concentration increases from 2 wt% to 4 wt% while the average concentration remains constant, the local bath depth and local ACD decrease by about 1 cm if the superheat is constant.

The present treatment may be simplistic, since flow induced by density variations was not considered. There is a need for further studies of the dynamic behaviour of the metal-bath interface, starting with the Navier-Stokes equations.

4. A Statistical View on Anode-Cathode Distance and Current Efficiency

4.1 Current Efficiency at Low Anode-Cathode Distance

It was suggested earlier [9] that the excessive loss in CE at low ACD is caused by contact between metal waves and gas bubbles. Provided that the metal waves and the bubbles both have an average height and a standard deviation, the loss in CE will be related to the overlap between the metal and gas "bell curves". A simplistic model was used, assuming that the CE loss due to metal-gas contact is proportional with the area underneath the overlapping part of the curves. The Gaussian probability distribution was used for the metal as well as for the gas bubbles.

Figure 5 shows that the CE decreases abruptly when the ACD is below a certain limit. This is in accordance with industrial measurements [20]. It is probable that the gas bubbles at a slotted anode have smaller dimensions than the bubbles at a non-slotted anode, due to the shorter bubble travelling distance in the former case. Smaller bubbles will also produce smaller metal wave amplitudes. The two sets of data in Figure 5 may therefore be taken to represent a slotted anode (Case I) and a non-slotted anode (Case II).

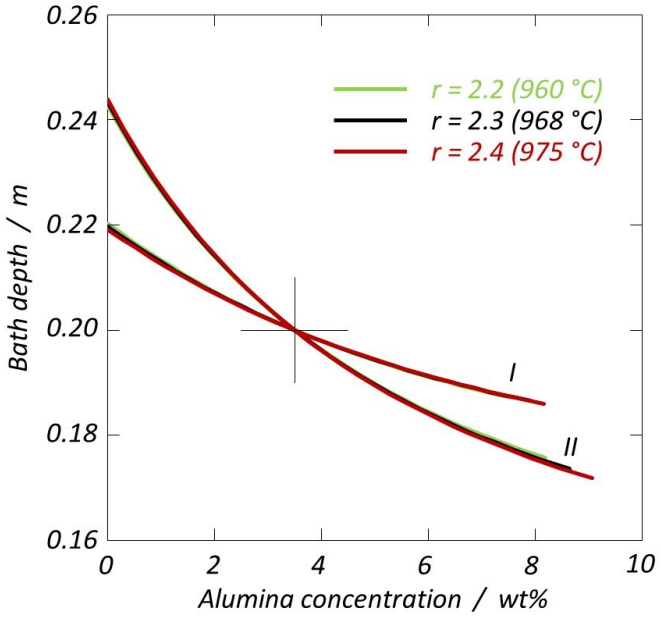

Figure 4. Local bath depth as a function of the local alumina concentration, calculated for three baths with different NaF/AlF_3 ratios (r) and 5 wt% CaF_2. The mean bath depth and alumina concentration were 0.2 m and 3.5 wt%, respectively. Curve I: At the liquidus temperature [19], Curve II: At fixed temperatures given in the figure.

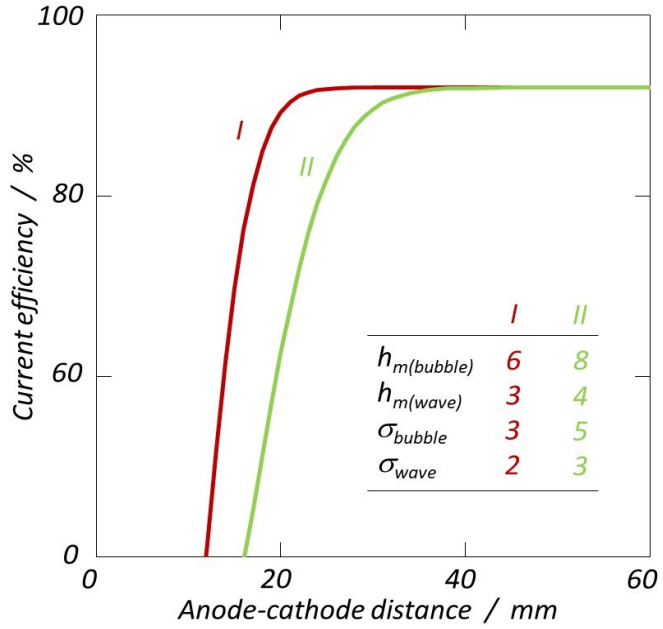

Figure 5. CE as a function of the ACD. The CE was taken to be 92 % when there is negligible overlap between bubbles and metal waves. The average height (h_m, mm) and the standard deviation (σ, mm) for waves and bubbles are given in the figure. Case I and Case II may be taken to represent a slotted anode and a non-slotted anode, respectively.

4.2 Current Efficiency and Anode-Cathode Distance Distribution

The data in Figure 5 was applied for calculation of the CE as a function of the standard deviation in ACD and the mean ACD. The Gaussian probability distribution was applied. As shown in

Figure 6, the CE decreases if the variation in ACD is too large. The reason is that a very non-uniform ACD implies that a higher number of anodes operate at very low ACD where the CE is low. The effect of non-uniformity is more severe at low average ACD, which means that modern high productivity cells are more vulnerable. Further productivity increase may then require actions to reduce the standard deviation in the ACD.

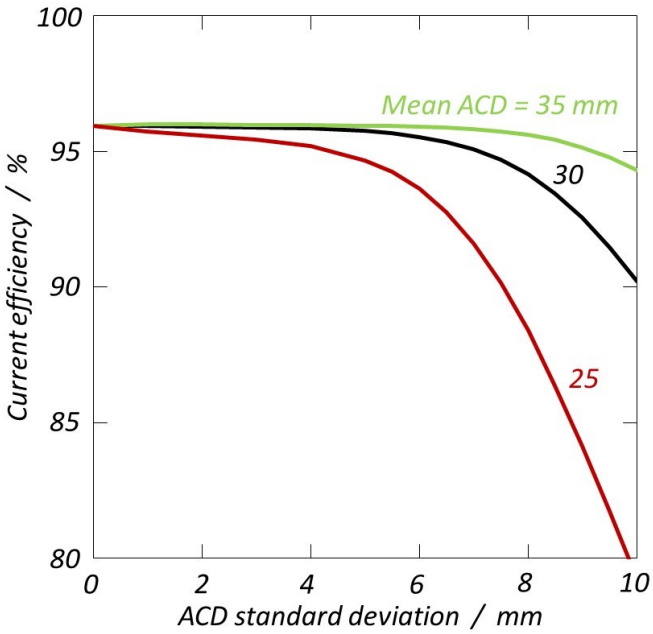

Figure 6. Current efficiency as a function of the standard deviation in the ACD at three different mean ACDs as shown in the figure. Gaussian ACD probability distribution, calculations based on extra CE loss due to bubble-metal collisions as in Case I in Figure 5.

5. Discussion

One way to attack the problem of alumina non-uniformity would be the introduction of variable alumina feeding, i.e., controlling the individual feeders according to the actual situation in the cell. In its simplest form, the individual feeding rates could be independent of the anode cycle, but different for each feeder. This was introduced in a Hydro smelter [8], which entailed reduced AE frequency, increased CE, reduced number of anode spikes, and fewer anode adjustments after setting. One step further would be the development of anode cycle dependent feeding, i.e., that the individual feeding rates would be determined according to the anode cycle. This requires a reliable and verified bath flow and alumina consumption model that accounts for which anodes were recently set. Such models are currently within reach. As an even more advanced option, the individual feeders could be controlled based on monitoring the anodic current distribution. Controlling the alumina distribution will, of course, work better in a cell with many feeders. More efficient feeders, i.e., feeders that allow a larger proportion of the alumina batch to be dispersed as individual alumina particles, should always be on any aluminium company's wish-list.

Uniform alumina concentration may also relieve non-uniform ACD caused by bath density variations, but there will still be metal surface perturbations caused by Lorentz forces. It is technically possible to apply individual anode regulation based on individual anode current monitoring, but the method is probably too expensive.

Putting an end to anode replacements would largely eliminate ACD variation caused by Lorentz forces as well as changes in bath density, but variation related to sludge or bottom ledge may not be eliminated. Several patents concerning continuous prebaked anodes have been filed in the past (e.g., see refs. [21-23]). Even though the use of continuous anodes in modern cells has not been considered successful, it should be mentioned that such anodes were operated for more than 20 years at Rheinwerk, Germany [24], indicating that the technology is not entirely impracticable. Maybe it's time to wipe off the dust from the concept of continuous prebaked anodes?

6. Acknowledgement

This paper was largely based on past and current projects financed by the Research Council of Norway and Hydro Aluminium.

7. References

1. Pascal Lavoie and Mark P. Taylor, Alumina concentration gradients in aluminium reduction cells, *Advances in Molten Slags, Fluxes, and Salts: Proceedings of the 10th International Conference on Molten Slags, Fluxes and Salts (MOLTEN16)*, TMS 2016, 791-797.
2. Xiping Chen, Wangxin Li, Yanzang Zhang, Shilin Qiu, and Chris Bayliss, Investigation on formation mechanism of non-anode effect related PFC emissions from aluminum reduction cells, *Light Metals* 2013, 877-881.
3. Jayson Tessier, Katie Cantin, and David T. Magnusson, Investigation of alumina concentration gradients within Hall-Héroult electrolytic bath, *Light Metals* 2018, 515-522.
4. International Aluminium (retrieved June, 2022), https://international-aluminium.org/statistics/perfluorocarbon-pfc-emissions/
5. Wangxing Li, Qingyun Zhao, Jianhong Yang, Shilin Qiu, Xiping Chen, Jerry Marks, and Chris Bayliss, On continuous PFC emission unrelated to anode effects, *Light Metals* 2011, 309-314.
6. Luis Espinoza-Nava, Christine Dubois, and Eliezer Batista, Method development to estimate total low voltage and high voltage PFC emissions, *Light Metals* 2020, 758-765.
7. Asbjørn Solheim and Bjørn P. Moxnes, Anodic current distribution in aluminium electrolysis cells, *Aluminium of Siberia*-2007, Krasnoyarsk, Russia, September 11-13, 2007 (Proceedings, 21-27).
8. Bjørn Moxnes, Asbjørn Solheim, Morten Liane, and Anveig Halkjelsvik, Improved cell operation by redistribution of the alumina feeding, *Light Metals* 2009, 461-466.
9. Asbjørn Solheim, Current efficiency in aluminium reduction cells: Theories, models, concepts, and speculations, *Light Metals* 2014, 753-758.
10. Asbjørn Solheim, Reflections on the low voltage anode effect in aluminium electrolysis cells, *Light Metals* 2022, 971-978.
11. Jomar Thonstad, Sverre Rolseth, and Rudy Keller, On the mechanism behind low voltage PFC emissions, *Light Metals* 2013, 883-885.
12. Steinar Kolås, Phillip McIntosh, and Asbjørn Solheim, High frequency measurements of current through individual anodes: Some results from measurement campaigns at Hydro, *Light Metals* 2015, 729-734.
13. Benoit Verreault and Renaud Santerre, Millivolt anodes – New technology opportunities for better pot control, Proceedings of 35th International ICSOBA Conference, Hamburg, Germany, 1-5 October 2017 (*Travaux* **46**, 823-833).
14. Jan Híveš, Jomar Thonstad, Åsmund Sterten, and Pavel Fellner, Electrical conductivity of molten cryolite-based mixtures obtained with a tube-type cell made of pyrolytic boron nitride, *Light Metals* 1994, 187-194.

15. Martin Segatz, Christian Droste, and Detlef Vogelsang, Magnetohydrodynamic effect of anode set pattern on cell performance, *Light Metals* 1997, 429-436.
16. Jinsong Hua, Pascal Beckstein, Eirik Manger, Steinar Kolås, Øyvind Jensen, and Sigvald Marholm, Numerical modeling of anode changes and their effect on current distribution and magnetohydrodynamic behavior of an aluminium reduction cell, *Light Metals* 2024, 481-492.
17. Asbjørn Solheim, The Density of Molten NaF-LiF-AlF_3-CaF_2-Al_2O_3 in aluminium electrolysis, *Aluminum Transactions* **2**(1) 161-168 (2000).
18. J.D. Edwards and T.A. Moorman, Density of aluminum from 20 °C to 1000 °C, *Chem. & Met. Eng*. **24** 61-64 (1921).
19. Asbjørn Solheim, Sverre Rolseth, Egil Skybakmoen, Lisbet Støen, Åsmund Sterten, and Trond Støre, Liquidus temperatures for primary crystallization of cryolite in molten salt systems of interest for the aluminium electrolysis, *Met. Trans. B* **27B,** 1996, 739-744.
20. Sverre Rolseth, Tugrul Muftuoglu, Asbjørn Solheim, and Jomar Thonstad, Current efficiency at short anode-cathode distance in aluminium electrolysis, *Light Metals 1986*, 517-523.
21. Julian L. Reynolds (Reynolds Metals Company), Anode for alumina reduction cells, US Patent No. 2,958,641 (1960).
22. Hans K. Holmen, Tormod Naterstad, Jan Hurlen, and Sigmund Gjørven (Hydro), Aluminum electrolysis cell with continuous anode, US Patent No. 5,071,534 (1991).
23. Drago D. Juric (Comalco), Continuous prebaked anode cell, US Patent No. 5,665,213 (1997).
24. Detlef Vogelsang, Ingo Eick, Martin Segatz, and Christian Droste, Retrofit of VAW Rheinwerk, Part I: Modernization concept, *Light Metals* 1997, 233-238.